Diverse organic carbon dynamics captured by radiocarbon analysis of distinct compound classes in a grassland soil

Katherine E. Grant[1][*], Marisa N. Repasch[1,2,3], Kari M. Finstad[1], Julia D. Kerr[1], Maxwell Marple[1], Christopher J. Larson[1,4], Taylor A. B. Broek[1], Jennifer Pett-Ridge[1,5], and Karis J. McFarlane[1]

[1]Physical and Life Sciences Directorate, Lawrence Livermore National Laboratory, Livermore, CA 94550, USA
[2]Institute of Arctic and Alpine Research, University of Colorado, Boulder, CO, USA
[3]Earth and Planetary Sciences, University of New Mexico, Albuquerque, NM, USA
[4]Department of Earth and Environmental Science, University of Pennsylvania, Philadelphia, PA, USA
[5]Life and Environmental Sciences Department, University of California-Merced, Merced, CA, USA

Correspondence to: Katherine E. Grant (grant39@llnl.gov)

Supplementary Material

1 Density Separation

To fully characterize the soil samples from the Hopland site, we compared the compound class measurements and the physical fractionations to a separate SPT density separation experiment as well as a "bulk" ^{13}C nuclear magnetic resonance (NMR) experiment to compare the change in chemical structure in <2mm soils.

1.1 Methods

Bulk soil samples (~20 g) were density fractionated using a low C and N sodium polytungstate (SPT-O, Geoliquids) into three density fractions: the free light fraction (FLF), the occluded light fraction (OLF), and the dense fraction (DF) according to the method in [*McFarlane et al.*, 2013], The density separation was done in triplicate for each depth sample. The separation density was 1.65 g mL^{-1}. For the experiment all glassware was pre-combusted to reduce C contamination.

For our heavy liquid we used 850 g of SPT powder in 825 g of 18.2 ΩM water in a 1 L beaker and was constantly stirred using a stir bar. Repeat measurements of the SPT solution ensured the correct density of 1.65 g mL^{-1}.

30   For each replicate, 20 grams of 2 mm sieved soil from each depth (0-10 cm, 10-20 cm,

31   20-50 cm, and 50-100 cm) was transferred into an acid-washed centrifuge tube and 100ml of

32   SPT-0, the tube was inverted by hand ensuring the entire sample was in contact with the SPT.

33   The samples were centrifuged at 3500 rpm for 1 hour and the floating material was aspirated and

34   collected via vacuum filtration. Samples were washed repeatedly through a Pall Supor 0.45 mm

35   47 mm PES filter using 18.2 MΩ water. The FLF was dried in a 65˚C oven overnight, weighed,

36   and then transferred into a 105˚C oven overnight. Once cooled, samples were ground with a

37   mortar and pestle.

38   To recover the OLF fraction the centrifuge tubes were filled with 75ml SPT. The sample

39   was mixed using a benchtop mixer for 1 minute at 1400 rpm. The sample vial was then

40   transferred into an ice filled Styrofoam box where it cooled for 5 minutes and then sonicated for

41   1 minute at 80% amplitude. The samples were centrifuged at 3500 rpm for 1 hour to recover the

42   OLF. The floating material (OLF) was then aspirated into a side-arm flask and rinsed five times

43   with about 150 mL of 18.2 MΩ water. The samples were dried at a 65˚C overnight, weighed, and

44   then transferred to a 105˚C oven overnight. The sample was then ground using a mortar and

45   pestle and transferred into vials for later analysis.

46   The remaining SPT was then aspirated from the centrifuge bottles, leaving just the

47   residual DF. The DF was rinsed until the density of the supernatant reached 1g/ml. The samples

48   were dried in a 65˚C oven overnight, weighed, and then transferred to a 105˚C oven overnight.

49   The DF was grinded using a ball mill and transferred into vials for later analysis.

50   This entire process was performed in triplicate for each depth; four depths, twelve samples.

51   As described above, each of the fractions (FLF, OLF, and DF) was loaded into quartz tubes

52   for ^{14}C analysis, and foil balled for δ^{13}C analysis.

53

1.2 Results:

To compare our size fractionated samples to a traditional density fractionation, we carried out the

separated our <2mm "bulk soil" into three fractionations with a heavy liquid. The three fractions

were the free light fraction (FLF) or mineral free, the occluded light fraction (OLF) is also

mineral free, but is found in aggregates and requires disruptive (sonication) energy input, and the

dense fraction (DF) is the mineral associated fraction (Plaza et al. 2019). At each depth the FLF

was the youngest fraction and had roughly 26 %OC, the OLF by comparison generally is very

condensed with %OC ranging from 32 to 43%. The FLF ranged from +3 ± 5‰ in the surface to -

350 ±110‰ at depth. The OLF ranged from 18 ± 7 to -633 ± 21‰. The DF ranged from 14 ± 5

to -563 ± 9‰. In general, the DF was older than both the sand and <63 μm fractions at each

depth, suggesting some modern, mineral-free carbon is present in both the sand and silt/clay

fractions. While these separations are not perfect, they help us understand where most carbon is

concentrated within a sample. Generally, these HREC soils have very little FLF and OLF by

mass, the DF consists of 80% of the total carbon within the sample (SI Table). The HF includes

both the sand and silt/clay fractions. Because our >63μm fraction has younger $\Delta^{14}C$ values than

the <2mm to >63μm or DF fractions we can assume the <63μm fraction includes free particulate

carbon which cycles faster than the truly mineral-associated DF. The OLF is older than both the

DF and the FLF at the deepest depth, which could mean aggregation is a mechanism for greater
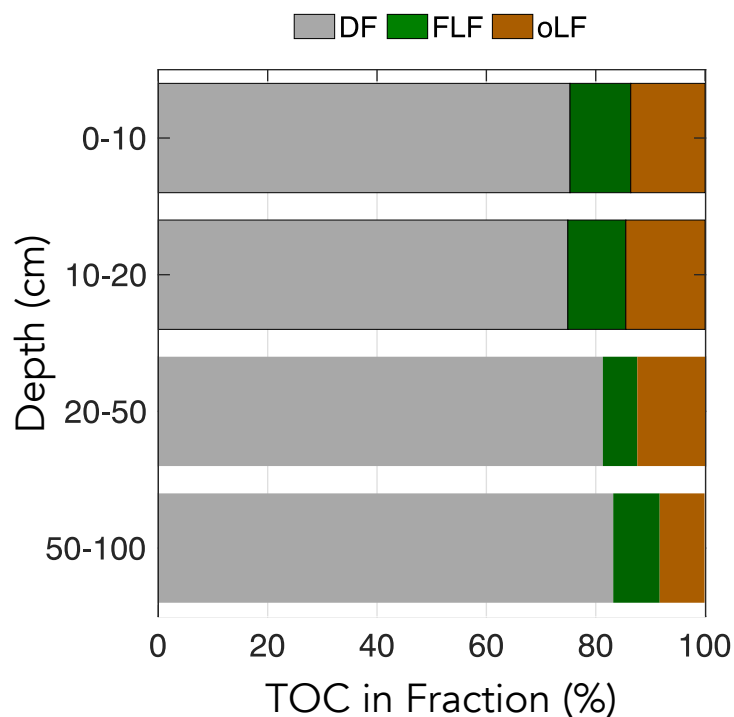
stability in these soils.

Figure S2. A. Density separation radiocarbon results for the FLF, OLF, and DF.B. fraction of OC contained in each density fraction. Error bars represent standard error on triplicate experiment measurements.

2 Nuclear Magnetic Resonance (NMR) Spectroscopy

2.1 Methods

Semi-quantitative solid-state cross polarization magic angle spinning (CPMAS) ^{13}C NMR was performed on a depth profile of <2mm soil horizon samples to identify target compound classes. In order to reduce paramagnetic iron interferences, soil samples were first de-mineralized using 2% hydrofluoric acid (HF) following the protocols of [*Sanderman et al.*, 2017]. Approximately 0.5 g of de-mineralized soil was crushed into a fine powder with an agate mortar and pestle and loaded into a 7.5mm rotor for NMR analysis. ^{13}C-NMR spectra were collected on a Bruker Neo

86 console operating at a Larmor frequency of 75.71 MHz and externally referenced to adamantane

87 (δ=38.48 ppm). [1]H-^{13}C cross polarization measurements were collected while spinning at 6 khz

88 with a contact time of 1ms and a recycle delay of 2s. Spectra were acquired with between

89 115518 and 346996 scans depending on sample organic carbon concentration. Spectral intensity

90 was normalized by mass and number of scans in Matlab. This method allows for direct

91 comparison between the spectra measured with the same parameters. Spectra were processed

92 with Bruker Topspin software and peak integrations were done with Matlab (vR2022b). Data

93 was categorized by the following functional group shifts: 210-165 ppm, 165-145 ppm, 145-95

94 ppm, 95-52 ppm, 52-0 ppm, which correspond to C=O groups, aromatic C-O groups, other

95 aromatics and olefinics, O- and N-alkyl groups, and alkyl carbon groups respectively [*Baldock et*

96 *al.*, 2004; *Mao et al.*, 2017].

2.2 Results:

98 NMR spectra and total soil organic carbon content were collected from< 2 mm

99 hydrofluoric acid-rinsed soil samples (Figure 2). Total carbon declined from 3.4% at the surface

100 to 0.2% in the 50-100cm interval, with the steepest decline between the 0-10 and 10-20cm

101 intervals. The normalized relative abundances of the five molecular classes we identified by [13]C-

102 NMR are listed in Table 1. Generally, the magnitude of all peaks decreased between the surface

103 and subsurface soils, and the 50-100 cm depth had no detectable peaks over baseline. The

104 aromatic peak had the least decline within the sample set, with over 60% of the initial peak

105 intensity retained throughout the depth profile. By comparison, the 20-50 cm depth had >75%

106 less alkyl C relative to the surface soil. We note that the radiocarbon values between the de-

107 mineralized (hydrofluoric acid-rinsed) soils and bulk soils indicate a slightly older value in the

108 de-mineralized soil (SI Table 1), which suggests that some younger, highly labile carbon was
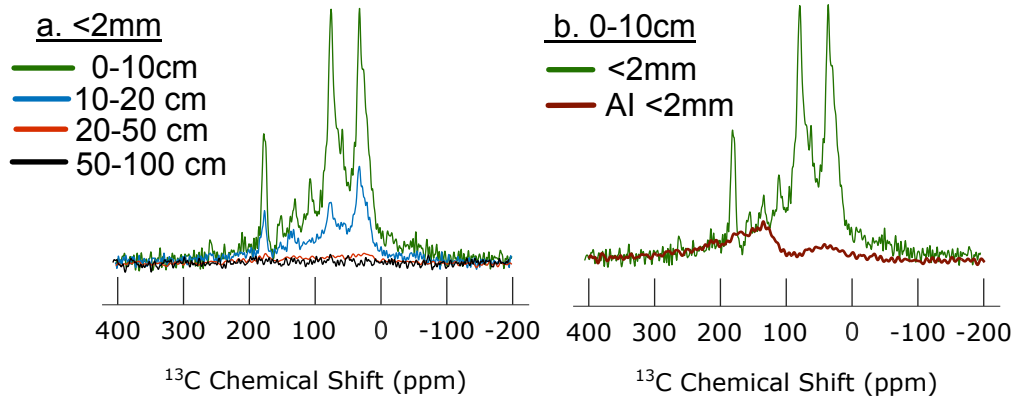
109   removed during this procedure.

110

111

112

113   Figure S4: (A) Soil state ^{13}C-NMR and characterization of bulk (< 2 mm) hydrofluoric acid-

114   treated soil collected from four depths of an annual grassland in Hopland, CA. Total organic

115   carbon was calculated separately on three physical size fractions at each depth. (B). Direct

116   comparison of NMR from AI fraction and bulk soil.

117

3.1 Radiocarbon Blank Assessment Method

119   To calculate the amount of exogenous C added during WEOC, TLE, and AA extractions,

120   process blanks were carried out independently. Blank analysis for compound specific

121   radiocarbon analysis (CSRA) becomes increasingly important when the extraction preparations

122   are complex and the sample size of the target compound is small [*Sun et al.*, 2020]. We used ^{14}C

123   modern and dead standard materials to quantify the excess C acquired through each extraction

124   procedure. For the acid insoluble fraction and untreated soil samples background corrections, we

125   ran ^{14}C-free coals as is standard at CAMS.

126   For the TLE extraction, an empty ASE cell was extracted by the same method as the soil

127   samples. A known amount of modern or dead ^{14}C materials was added to the dried down "blank

128   sample" in the quartz tube. This method uses the "indirect blank" calculation, using a

129   comparison of fraction modern (F^{14}C) to an accepted value, because there is not enough excess

130   carbon to measure the blank directly [*Santos et al.*, 2010]. For the AA blank analysis, a ^{14}C-dead

131   alanine powder and a ^{14}C-modern commercial protein powder were digested and processed

132   through the resin column following AA procedures.

133   In total, three ^{14}C-modern and nine ^{14}C-dead samples were analyzed to quantify the AA

134   blank (SI Table). For the TLE blank quantification, four ^{14}C-modern and four ^{14}C-dead samples

135   were analyzed. The size and F^{14}C of the blank were then determined using the methods and

136   published R script from Sun et al. (2020). The R script was run in R Studio version 4.1.2 (R Core

137   Team, 2021). Briefly, a Bayesian model was used to fit thousands of linear regression lines

138   between the F^{14}C and inverse of the sample size (1/ μg C), allowing for the calculation of the

139   F^{14}C and size of the blank, as well as their associated uncertainties.

140   *3.2 Radiocarbon blank assessment Results*

141   Extraneous C was quantified for the TLE and AA extractions (SI Table 4). The TLE blank

142   is 8.16 ± 2.54 μg of C with an F^{14}C value of 0.671± 0.252. The exogenous C added from the AA

143   extraction procedure is 11.934 ± 6.205 μg of C with F ^{14}C value of 0.807 ± 0.389. The WEOC

144   blank contribution is 2.818 ± 0.753 with a F^{14}C value of 0.298 ± 1.22 (details reported in Finstad

145   et al., 2023). Generally, the extracted ^{14}C samples were large enough (> 250 μg C) that the

146   contribution of the blank did not significantly shift the ^{14}C values outside the variability of

147   sample replicates. Future efforts will identify the source of extraneous C to lower this blank

148   contribution from materials or a methodology step and increase the applicability of this method

149   for smaller and more ^{14}C-depleated samples.

150   *4 Works Cited*

151

152   Baldock, J. A., C. A. Masiello, Y. Gélinas, and J. I. Hedges (2004), Cycling and composition of
153   organic matter in terrestrial and marine ecosystems, *Marine Chemistry*, *92*(1), 39-64,
154   doi:https://doi.org/10.1016/j.marchem.2004.06.016.
155   Mao, J., X. Cao, D. C. Olk, W. Chu, and K. Schmidt-Rohr (2017), Advanced solid-state NMR
156   spectroscopy of natural organic matter, *Progress in Nuclear Magnetic Resonance Spectroscopy*,
157   *100*, 17-51, doi:https://doi.org/10.1016/j.pnmrs.2016.11.003.
158   McFarlane, K. J., M. S. Torn, P. J. Hanson, R. C. Porras, C. W. Swanston, M. A. Callaham, and
159   T. P. Guilderson (2013), Comparison of soil organic matter dynamics at five temperate
160   deciduous forests with physical fractionation and radiocarbon measurements, *Biogeochemistry*,
161   *112*(1), 457-476, doi:10.1007/s10533-012-9740-1.
162   Sanderman, J., M. Farrell, P. I. Macreadie, M. Hayes, J. McGowan, and J. Baldock (2017), Is
163   demineralization with dilute hydrofluoric acid a viable method for isolating mineral stabilized
164   soil organic matter?, *Geoderma*, *304*, 4-11, doi:https://doi.org/10.1016/j.geoderma.2017.03.002.
165   Santos, G. M., J. R. Southon, N. J. Drenzek, L. A. Ziolkowski, E. Druffel, X. Xu, D. Zhang, S.
166   Trumbore, T. I. Eglinton, and K. A. Hughen (2010), Blank Assessment for Ultra-Small
167   Radiocarbon Samples: Chemical Extraction and Separation Versus AMS, *Radiocarbon*, *52*(3),
168   1322-1335, doi:10.1017/S0033822200046415.
169   Sun, S., et al. (2020), 14C Blank Assessment in Small-Scale Compound-Specific Radiocarbon
170   Analysis of Lipid Biomarkers and Lignin Phenols, *Radiocarbon*, *62*(1), 207-218,
171   doi:10.1017/RDC.2019.108.
172